Development and evaluation of a physico-biochemical model for Escherichia coli in bathing waters

Wang, Hao; Blauw, Anouk; van Gils, Jos; Boelee, Eline; Sylvestre, Émile; Medema, Gertjan

DOI
10.1016/j.watres.2025.125199

Publication date
2025

Document Version
Final published version

Published in
Water Research

Water Research 291 (2026) 125199

Contents lists available at ScienceDirect

Water Research

journal homepage: www.elsevier.com/locate/watres

Development and evaluation of a physico-biochemical model for *Escherichia coli* in bathing waters

Hao Wang [a,b,*], Anouk Blauw [a], Jos van Gils [a], Eline Boelee [a], Émile Sylvestre [b,c], Gertjan Medema [b,c]

[a] Deltares, MH Delft 2600, the Netherlands
[b] Water Management Department, Faculty of Civil Engineering and Geosciences, Delft University of Technology, Stevinweg 1, Delft, CN 2628, the Netherlands
[c] KWR Water Research Institute, Groningenhaven 7, Nieuwegein, PE 3433, the Netherlands

HIGHLIGHTS

- We developed a new generic physico-biochemical model for fecal bacteria.
- We validated and evaluated the model for *Escherichia coli* in estuarine and coastal waters.
- Including UVA and UVB photo-inactivation improves *E. coli* die-off predictions.
- Photo-inactivation is significant in clean waters but less significant with high CDOM.
- Sediment composition should be considered when predicting peaks in turbid waters.

GRAPHICAL ABSTRACT

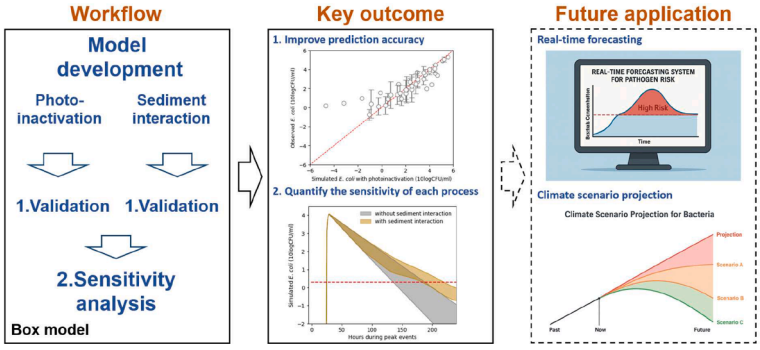

ARTICLE INFO

Keywords:
Fecal bacteria
Water quality modelling
Photo-inactivation
Sediment interaction

ABSTRACT

The risk of infection by enteric pathogens in bathing waters is generally monitored by using fecal indicator bacteria (FIB). Mechanistic models are efficient tools to predict FIB concentrations in bathing waters, both in near-future forecasting and in long-term climate change projections. However, most existing mechanistic FIB models are limited by the availability of observations for validation and incorporation of all relevant physical, biological, and chemical (physico-biochemical) processes. Therefore, the quantitative influence of different physio-biochemical processes and impact factors is missing. To enhance the understanding of FIB fate in different aquatic systems, we developed a comprehensive yet generically applicable physico-biochemical model, focused on *Escherichia coli* (*E. coli*). It includes a die-off module and a sediment interaction module. Separate validation of the two sub-modules demonstrated the reliability of our modeling approach. The die-off module shows a higher R^2 value (0.88) and lower RMSE value (1.1 day^{-1}) than the existing models (0.48–0.79, and 1.8–7.2 day^{-1}). This demonstrated an improvement by adding Ultraviolet-A and Ultraviolet-B (UVB) inactivation and UV spectrum extinction due to colored dissolved organic matter (CDOM) absorption. According to our sediment module validation, considering the impact of sediment composition on *E. coli* attachment can improve the allocation of *E. coli* between waters and sediments. Sensitivity analysis showed that 1) photo-inactivation is important in low CDOM waters, but not in high CDOM waters, where the UV penetration is limited; 2) the impact of sediment

* Corresponding author.
E-mail address: hao.wang@deltares.nl (H. Wang).

https://doi.org/10.1016/j.watres.2025.125199
Received 21 August 2025; Received in revised form 12 December 2025; Accepted 15 December 2025
Available online 16 December 2025

interaction can extend the duration of a peak event in high turbid waters. This work demonstrated the dominant impact factors in different aquatic systems for *E. coli* prediction. The new generic model enables better simulation of bathing water quality across different types of aquatic environments, which can be a useful tool to inform management at bathing sites. Future applications can choose processes selectively from the new FIB physico-biochemical model and couple it with appropriate hydrological/hydrodynamic models to address specific environmental conditions and research purposes.

1. Introduction

Waterborne pathogens at bathing sites, originating from wastewater treatment plant effluents, agricultural runoff, combined sewer overflows, and sewer leakages or septage, pose a significant public health risk. The EU Bathing Water Directive (EU, 2006) regulates recreational bathing water quality based on biweekly fecal indicator bacteria (FIB) monitoring, such as *E. coli* and *Enterococcus*. However, this frequency may not be sufficient for capturing peak events due to rapid changes in FIB concentrations (Jozić et al., 2024). High-frequency monitoring is costly, and sample transport and the standard enumeration method introduce time lags that limit early warning (Enns et al., 2012). FIB modeling helps address these gaps and enables near-future forecasting and the impacts of climate change on bathing water quality (King et al., 2021; Sterk et al., 2013).

Current FIB prediction models mainly target rural catchments and sub-catchments and typically operate at a daily timestep (De Brauwere et al., 2014a; Kim et al., 2017; Ouattara et al., 2013; Tong et al., 2024; Worku Meshesha et al., 2020). They generally comprise three components: 1) an emission module estimating FIB sources to aquatic systems; 2) a physico-biochemical module describing in-system physico-biochemical processes of FIB; and 3) a hydrology/hydrodynamics module simulating horizontal and vertical transport. The emission and hydrological module components are typically site-specific, but the physico-biochemical processes tend to be consistent across aquatic environments (Cho et al., 2016; de Brauwere et al., 2014b). To study FIB fate and transport across various water types—from land to sea in both urban and rural settings—a universally applicable physico-biochemical FIB module is needed (Hipsey et al., 2008). However, recent review studies (Cho et al., 2016; Nelson et al., 2018) suggested that the current models lack sufficient details in photo-inactivation and sediment interaction, which are the key processes alongside Natural die-off (die-off in darkness) (de Brauwere, 2014).

Photo-inactivation can have a strong impact on the FIB die-off. UV disinfection is widely used in waste stabilization ponds and constructed wetlands (Silverman and Guest, 2022; Zhang et al., 2019). Sunlight inactivates FIB via two mechanisms: 1) endogenous damage, triggered by absorbing photons in the UVB and UVA (280 – 400 nm) range, and 2) exogenous damage, which needs external photosensitizers (e.g., natural organic matter) as media (Nelson et al., 2018). Given that shorter wavelengths have stronger effects on inactivation (Nelson et al., 2018), Photo-inactivation rates should reflect cumulative effects across the spectrum. However, the current FIB physico-biochemical models tend to simplify this mechanism (Cho et al., 2016), by ignoring the photo-inactivation impact (De Brauwere et al., 2014a; Kim et al., 2017; Ouattara et al., 2013; Thorndahl et al., 2024; Worku Meshesha et al., 2020) or by estimating it from a total radiation coefficient while also neglecting light extinction caused by colored dissolved organic carbon (CDOM) (Shi et al., 2024; Tong et al., 2024).

UV extinction is highly sensitive to water turbidity (Wang and Seyed-Yagoobi, 1994). CDOM is the dominant absorber for UV radiation in the ocean and inland waters (Kuhn et al., 1999; Laurion et al., 2000). CDOM are often adequate in FIB sources, like wastewater effluents and overflows (Gonsior et al., 2011; Kalev et al., 2021), and transport with FIB to bathing waters. Resuspension sediments from bather activities also reduce UV penetration (Graczyk et al., 2010). Therefore, CDOM and suspended sediment should be considered when calculating *E. coli* photo-inactivation. Given the clear positive relation between dissolved organic carbon (DOC) and CDOM concentrations in global aquatic environments (Fichot and Benner, 2011; Li et al., 2018), DOC concentration, which is easier to measure and commonly simulated in water quality models, can be used to estimate UV attenuation (Morris et al., 1995). To incorporate FIB photo-inactivation by the UVA+UVB spectrum into the new model, four steps need to be taken (Nelson et al., 2018): (1) characterizing the spectrum upon water surfaces; (2) estimating the spectrum extinction in waters; (3) predicting endogenous inactivation, and (4) exogenous inactivation. Since *E. coli* is not noticeably susceptible to exogenous inactivation (Nguyen et al., 2015), the fourth step is omitted in this study.

Sediment serves as a reservoir for FIB in both fresh and marine waters (Fluke et al., 2019; Labite et al., 2010; Pachepsky and Shelton, 2011). To capture this, some FIB physico-biochemical models incorporate the sediment interaction, including attachment-detachment, sedimentation, resuspension, and hyporheic exchange (Kim et al., 2010, 2017; Shi et al., 2024; Thupaki et al., 2013). In most previous modeling studies, the attachment between FIB and suspended sediment is irreversible and determined by a constant partitioning rate, ignoring the positive relation between suspended sediment concentration and attached FIB (Garcia-Armisen and Servais (2009). More recent approaches adopt a dynamic partitioning rate, based on suspended sediment concentrations and a constant partitioning coefficient (K_{SS}), representing the absorption capacity of suspended sediment per unit to FIB (Bai and Lung, 2005; Gao et al., 2011; Thupaki et al., 2013). Nevertheless, the partitioning coefficients were valued arbitrarily in a range of 0.01 – 10 $m^3\ g^{-1}$. Kim et al. (2010, 2017) pointed out that the partitioning coefficient, as an intrinsic character determined by suspended sediment composition, is a function of the clay proportion in total suspended sediments (TSS). Incorporating this function in the model requires detailed TSS dynamics. Fortunately, given the progress of TSS simulation in current water quality models, this can be tackled by coupling the FIB physico-biochemical module with an existing TSS module.

This study aims to develop a generic mechanistic FIB model incorporating the latest understanding of *E. coli* physico-biochemical processes. While the model is developed and validated based on *E. coli* data, it can be adapted to other fecal bacteria and viruses by reparameterization. Compared to the existing models, the new model 1) considers the photo-inactivation due to the UVA+UVB spectrum, in which extinction caused by CDOM and TSS is included; 2) introduces a dynamic K_{SS} based on clay and non-clay sediment fractions. By comparing with observations from previous studies, the new functions have been validated individually via a box model. The sensitivity of the impact factors in different types of aquatic ecosystems was evaluated via sensitivity analysis. By coupling with a specific emission module and hydrology/hydrodynamics module, this new FIB model can be widely applied for FIB predictions in various water systems.

2. Materials and methods

In this study, we first developed a new generic module representing key processes affecting *E. coli* in surface waters (Section 2.1). The module was developed within Delwaq: the water quality model within the Delft3D-WAQ modelling framework (Deltares, 2020), which is based on the advection-diffusion-reaction equation. We then applied a box

model for model validation with literature data and sensitivity analysis. The box model functions as a single grid cell of 3D hydrodynamic models (Fig. 1b). It can reproduce site-specific conditions for different environments by choosing different input data: either from literature or from existing 3D model applications. By comparing with observations time, the box model enables efficient test, calibration, validation and stochastic analysis under varying hydrodynamic scenarios.

Temperature and salinity are commonly and validation data from literature (Maraccini et al., 2016; Nguyen et al., 2015), we compared the new module with two existing model descriptions in Delwaq and in SWAT (Section 2.2). We also assessed the sensitivity of *E. coli* die-off rates using boundary conditions from two 3D models representing different aquatic systems (Section 2.3). Table 1 summarizes the simulation time, activated modules and impact factors for model comparison and the sensitivity analysis scenarios. The impact factors we considered in the study include temperature, salinity, radiation, DOC concentration, and sediment concentration and composition.

2.1. FIB physico-biochemical model development

As shown in Fig. 1a, *E. coli* die through photo-inactivation and natural die-off. To represent the sediment interaction, we defined three bacterial states: 1) unattached *E. coli* in the water column; 2) attached *E. coli*; 3) sedimented *E. coli*, either in pore water or in deposited sediment. These *E. coli* states can transfer via attachment-detachment, deposition, resuspension, and hyporheic exchange.

E. coli die-off is modeled by a total die-off rate (k_{tot}, h^{-1}) that combines natural die-off in darkness (k_{dark}, h^{-1}) and endogenous photo-inactivation (k_{photo}, h^{-1}). k_{dark} is determined by temperature and salinity (Chan et al., 2015). Details are provided in the supplementary information **(SI 1.1)**.

$$k_{tot} = k_{dark} + k_{photo} \quad (1)$$

The total die-off applies to unattached bacteria. For attached and sedimented bacteria, photo-inactivation was excluded, and temperature and salinity effects were reduced by 50 % and 90 %, respectively, due to sediment protection (Garzio-Hadzick et al., 2010). Key equations, parameters and sources are shown in 2.1.1–2.1.3 and Table S1, with model inputs and outputs listed in Table S2.

2.1.1. Endogenous photo-inactivation

To estimate photo-inactivation, we first derived the UVA + UVB spectrum from the total global solar radiation (TGSR). We used a constant UVA + UVB fraction ($f_{UVA+UVB}$) and standard UV spectra ($E_{st_{1.05}}(\lambda)$ and $E_{st_{1.5}}(\lambda)$ (Kirk, 1981; (Annually, 1995), **Figure S1**) to redistribute the intensities across 300 – 400 nm. T_{air_mass} is a temperature sensitivity coefficient for air mass given by (https://www.knmi.nl/over-het-knmi/nieuws/lichte-lucht-zware-lucht, **Figure S2, Table S1**).

$$E_0(0,\lambda) = TGSR \times f_{UVA+UVB} \times f(\lambda) \quad (2)$$

$$f(\lambda) = \frac{\left(E_{st_{1.05}}(\lambda) + E_{st_{1.5}}(\lambda)\right) \times T_{air\_mass}}{\sum_{\lambda=300}^{400}\left[\left(E_{st_{1.05}}(\lambda) + E_{st_{1.5}}(\lambda)\right) \times T_{air\_mass}\right]} \quad (3)$$

The second step was estimating UV penetration with depth (z, m), since CDOM is the main UV absorber in natural waters (Bricaud et al., 1981; Zhang et al., 2020). The total diffuse attenuation coefficient ($K_{tot}(\lambda)$, m^{-1}) was calculated as the sum of CDOM attenuation coefficient ($K_{CDOM}(\lambda)$, m^{-1}), backscattering coefficient of inorganic suspended sediment ($b_{scatter}$, m^{-1}), and inherent attenuation coefficient of pure water ($K_{pure}(\lambda)$, m^{-1}).

Table 1
Different scenarios in model comparison and sensitivity analysis.

	Name	Simulation time	Active module	Active factors	Model source
Model comparison	M0	10 days	Die-off	T, S, I, DOC	This study
	M1	10 days	Die-off	T	SWAT
	M2	10 days	Die-off	T, S, I	Delwaq
Sensitivity analysis	S1	1 year	Die-off	T, S	This study
	S2	1 year	Die-off	T, S, I	This study
	S3	1 year	Die-off	T, S, I, DOC	This study
	S4	1 year	Die-off + sediment interaction	T, S, I, DOC, K_{SS_C}*	This study
	S5	1 year	Die-off + sediment interaction	T, S, I, DOC, K_{SS_D}*	This study
	E1	250 h	Die-off	T, S	This study
	E2	250 h	Die-off	T, S, I	This study
	E3	250 h	Die-off	T, S, I, DOC	This study
	E4	250 h	Die-off + sediment interaction	T, S, I, DOC, K_{SS_D}*	This study

*Note: K_{SS_C} and K_{SS_D} represent constant and dynamic partitioning rates, respectively. The K_{SS_C} value is 0.01 $m^3\ g^{-1}$ (Bai and Lung, 2005; Gao et al., 2011; Thupaki et al., 2013). T, S, and I are temperature, salinity and radiation, respectively.

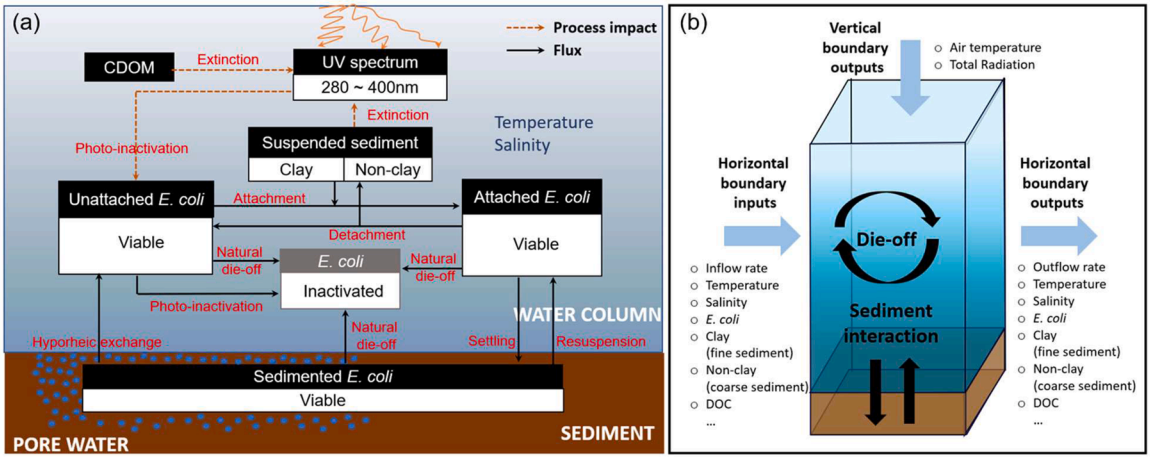

Fig. 1. Schematization of the FIB model (a) and the box model scheme with required boundary inputs (b). Photo-inactivation refers to damage via UV radiation; natural die-off includes various loss processes (e.g., predation, nutrient limitation). CDOM represents colored dissolved organic carbon.

$$E_0(z,\lambda) = E_0(0,\lambda) \times e^{K_{tot}(\lambda)\times z} \quad (4)$$

$$K_{tot}(\lambda) = K_{CDOM}(\lambda) + K_{pure}(\lambda) + b_{scatter} \quad (5)$$

$$b_{scatter} = \left(b^*_{clay} \times C_{clay} + b^*_{sand} \times C_{sand}\right) \times P_{back} \quad (6)$$

$E_0(0,\lambda)$ is the UV intensity at the water surface (W m^{-2}), $K_{pure}(\lambda)$ is calculated based on the studies of Morel et al. (2007); Smith and Baker (1981). b^*_{clay} and b^*_{sand} are the scattering coefficients of clay and sand (m^2 g^{-1}), respectively (Stramski et al., 2007); P_{back} (-) is the backscattering probability (Bi et al., 2023), $K_{CDOM}(\lambda)$ is modeled as an exponential decay function (Jerlov, 2014; Shifrin, 1998):

$$K_{CDOM}(\lambda) = A \times e^{-s_e\times\lambda} \quad (7)$$

Where, s_e (nm^{-1}) is a spectral slope parameter representing CDOM composition, with a recommended value of 0.015 (Bricaud et al., 1981; Jerlov, 2014; Shifrin, 1998; Twardowski et al., 2004). A, as an amplitude, reflects CDOM concentration. With the DOC concentration (C_{DOC}) and CDOM extinction coefficient ($K_{CDOM}(\lambda)$) in natural waters (rivers, lakes, coastal seas) from previous studies (Huovinen et al., 2003; Laurion et al., 2000; Morris et al., 1995; Scully and Lean, 1994), we developed a DOC–amplitude (A) relation (See 3.1). To make sure the relation is fitting for the UVA + UVB spectrum, only samples with more than three K_{CDOM} values across the spectrum were included **(SI)**.

The endogenous UV-induced reaction was calculated following Silverman and Nelson (2016). Details are in **SI 1.1**.

2.1.2. Attachment and detachment with suspended sediment

Bacterial attachment can be explicitly described by the extended Derjaguin-Landau-Verwey-Overbeek (DLVO) theory (van Loosdrecht et al., 1989). To simplify calculations and use commonly available input data, we adopted the "fast" attachment-detachment kinetics (Thupaki et al., 2013). These assume that attachment-detachment processes are faster than other processes, and masses of unattached and suspended-sediment attached *E. coli* are in equilibrium all the time (Bai and Lung, 2005; De Brauwere et al., 2014a; Gao et al., 2011).

$$fdf = \frac{C_{b,\ attach}}{C_{b,free} + C_{b,attach}} \quad (8)$$

$$fdf = \frac{C_{SS} \times K_{SS}}{1 + C_{SS} \times K_{SS}} \quad (9)$$

$$C_{SS} = C_{clay} + C_{non-clay} \quad (10)$$

Where, $C_{b,free}$ and $C_{b,attach}$ are the concentrations of unattached *E. coli* and suspended-sediment attached *E. coli* (CFU m^{-3}), respectively. *fdf* represents the partitioning rate (-), C_{SS} is TSS concentration (g m^{-3}). K_{SS} is the partitioning coefficient. Unlike a constant partitioning coefficient (K_{SS}, -), we defined it as a function of the percentage of clay (P_{clay}, %) in TSS (Kim et al., 2017).

$$K_{SS} = 10^{-1.6} \times \left(P_{clay}\right)^{1.98} \quad (11)$$

$$P_{clay} = \frac{C_{clay}}{\left(C_{clay} + C_{non-clay}\right)} \times 100\% \quad (12)$$

We distinguished clay (C_{clay}, g m^{-3}) and non-clay sediment ($C_{non-clay}$, g m^{-3}) by the settling velocities **(Table S1)**. The clay sediment represents fine sediment with higher *E. coli* attachment capacity than the coarser non-clay sediment.

2.1.3. Interaction with sediment

Kim et al. (2017) indicated that sedimentation, resuspension, and hyporheic exchange are essential processes of the interactions between FIB and sediment. We assumed the unattached bacteria have no settling velocity, while attached bacteria settle based on a weighted average settling velocity of two suspended sediments **(SI 1.2)**. Sedimentation and resuspension depend on shear stress. Hyporheic exchange is determined by sediment density, volumetric seepage velocity, and bacteria concentration in pore waters. Equations are detailed in the SI (**SI 1.2–1.4**). Sedimentation, resuspension and vertical transport of sediment were calculated by the Delwaq model (Deltares, 2020) and coupled with the sediment–bacteria interaction module.

2.2. Die-off module validation and comparison

Table 1 lists the die-off module comparison scenarios (M0-M2). M0 is the new die-off module. M1 only considers the impact of temperature (SWAT model, (Kondo et al., 2021)); M2 considers the impacts of temperature, salinity, and photo-inactivation rates, estimated from visible light (Delwaq model, (Chan et al., 2015; Tong et al., 2024)).

Our module requires DOC concentration as an input, but only few available datasets include DOC observations. This restricts the number of datasets for validation of our new module. We used a dataset (Table S3)from two field experiments in California: at Pillar Point Harbor, San Joaquin Marsh and Arroyo Burro Lagoon, representing marine, freshwater and brackish water, respectively (Maraccini et al., 2016; Nguyen et al., 2015). To construct a similar condition at these three locations, the box model used measured *E. coli*, DOC concentration, salinity, and water depth from these two field experiments as initial conditions, and records of air temperature and radiation from the National Weather Service (https://www.weather.gov/) as inputs. Given that the field experiments were in situ incubations, horizontal input was not considered here.

2.3. Sensitivity analysis

Temperature and salinity are commonly used in *E. coli* predictions. The new model added UV-induced inactivation, UV extinction and sediment interaction. To explore these new functions' effects (Table 1), we performed a sensitivity analysis by incrementally adding new impact factors to the base scenario (S1 and E1). Five long-term scenarios (S1 – S5) represented stable low-flow conditions: S1) die-off module only controlled by T (temperature) and S (salinity); S2) die-off module controlled by T, S, and I (radiation), without the extinction; S3) the complete die-off module, including extinction; S4) the complete die-off module plus sediment interaction module with a constant partitioning coefficient (K_{SS_C}); S5) the complete die-off module plus the complete sediment interaction module.

In addition, four short-term scenarios (E1 – E4, Table 1) for peak *E. coli* contamination events were performed. By increasing the input of *E. coli* concentration from 0 to 2.4 × 10^6 CFU $100ml^{-1}$ and lasting for three hours between hours 25th - 28th, an accidental *E. coli* injection due to a combined sewer overflow was reproduced. Then we checked the event duration (above 250 CFU $100ml^{-1}$, based on the EU Bathing Water directive). The peak *E. coli* concentration was a weighted average of literature values (Erichsen et al., 2006; Thorndahl et al., 2024) and the injection duration was based on the dilution efficiency of the box model. For the impact factors, E1–3 were the same as S1–3, while E4 considered sediment interaction (S5). S4 was omitted because the constant partitioning coefficient tends to overestimate *E. coli* flux from sediment resuspension orders of magnitude in natural waters (Section 3.3), which is not comparable to other scenarios.

The long- and short-term sensitivity analyses were performed using the box models with boundary inputs from two sites in the Netherlands, representing coastal (Katwijk) and estuarine (Scheldt) conditions (Table 2). Locations of the two sites are shown in Fig. 2a-c. The time series' horizontal boundary inputs covering one year with daily time resolution (see Table 2 and Figure S3) were derived from the output of two 3D models: the DCSM-FM North Sea model (Zijl et al., 2013) for the Katwijk site in 2006 and the Scheldt estuary model for the Scheldt site in 2014 (Stolte and Schueder, 2019) **(Figure S3)**. The bathing water areas

Table 2
General setup of the box models (time series at the boundary were taken from the North Sea model and the Scheldt model).

	Parameter	Unit	Katwijk	Scheldt
General setup	Initial *E. coli*	CFU 100ml^{-1}	400	
	Area	m^2	10,000	
	C_{DOC}	g m^{-3}	0.0	
	C_{clay}	g m^{-3}	0.0	
	C_{sand}	g m^{-3}	0.0	
Constant boundary	Flow	m^3 day^{-1}	0.5	
	E. coli	CFU 100ml^{-1}	400 (S1-S5)	
			0 or 2.4 × 10^6 (M1 – M4)	
Timeseries boundary	Temperature	°C	5.5 – 18.8	0.0 – 25.1
	Salinity	Ppt	26.1 – 31.1	2.0 – 10.2
	TGSR	W m^{-2}	4.2 – 318	5 – 322
	C_{DOC}	g m^{-3}	1.0 – 3.0	3.6 – 5.5
	C_{clay}	g m^{-3}	0.1 – 7.8	4.2 – 14.0
	C_{sand}	g m^{-3}	0.0 – 16.8	10.1 – 68.0
	Tau	Pa	0.0 – 0.8	0.0 – 0.7
	z	M	0.8 – 3.5	1.95 – 2.1

are normally shallower than two meters, however, the output of the nearshore shallow area (<2 m) in the two 3D models is not representative because of the spatial resolution. Therefore, we chose two meters (yearly average) to make sure the water level dynamics derived from the two sites are representative. The vertical boundary inputs, including air temperature and TGSR, were from KNMI (Koninklijk Nederlands Meteorologisch instituut, https://dataplatform.knmi.nl/).

The boundary inflow rate of the box model is determined based on an approximately 2.5-day residence time. The computational timestep is one hour, and the simulation times for each scenario are in Table 1. The first 5 simulation days serve as a spin-up.

2.4. Sediment interaction module validation

The validation of the sediment interaction module was also based on the two box models in Section 2.3. Observations of *E. coli* in waters and sediments by the enumeration method were collected from previous studies (Devane et al., 2020; Fluke et al., 2019; Kim et al., 2010; Labite et al., 2010; Pachepsky and Shelton, 2011). Since our model aims to be applied to natural surface waters, only observational locations in natural waters, such as rivers, lakes, and coastal seas, were included. S5 was run with a gradient of *E. coli* boundary concentrations (4 × 10^2, 4 × 10^3, 4 × 10^4, and 4 × 10^5 CFU 100ml^{-1}), and the simulated *E. coli* distributions between waters and sediments were compared with observations.

We also compared K_{SS_D} (S5) and K_{SS_C} (S4) with a value of 0.01 m^3 g^{-1}, which is widely used in previous modeling work (Bai and Lung, 2005; Gao et al., 2011; Thupaki et al., 2013). Hence, we had 16 simulations (2 areas × 4 input concentrations × 2 types of K_{SS}) in total for the sediment interaction module validation. Hereafter, each simulation is labeled as "scenario name + area", e.g., "S5_Katwijk".

3. Results and discussion

3.1. Photo-inactivation module

Since DOC data is more accessible than CDOM from observations and simulation in water quality models, using DOC concentration to calculate K_{CDOM} (attenuation coefficient of UV by CDOM, in eq. (7)) improves input accessibility. Therefore, we established a relation ($A = 179.6 \times C_{DOC}^{1.19}$) between the amplitude A (in eq. (7)), which is a proxy of CDOM abundance in waters, and DOC concentrations from literature (Fig. 3). This empirical relation enables K_{CDOM} calculation from DOC concentrations.

In most locations, our new die-off module (M0) captured the observed decline of *E. coli* concentrations in the field experiments by Maraccini et al. (2016) (Fig. 4). However, the predictions of Arroyo Burro – Winter I and San Joaquin Marsh – Winter I were relatively poor compared to others. As the UV spectrum prediction in eq. (2) matched observations well **(Figure S5)**, two possible factors may explain how the UV extinction calculation leads to these deviations.

Due to the insufficient input data for a multi-layer water column model, our modelling simulations have no vertical variation, meaning the model results represent homogenous shallow water. However, the error bars of the observed die-off rate, representing the ranges of *E. coli* concentration at different water layers between 2 cm and 99 cm, indicate heterogeneous vertical distributions. Contrarily, the samples from Arroyo Burro – Winter I and San Joaquin Marsh – Winter are only from a

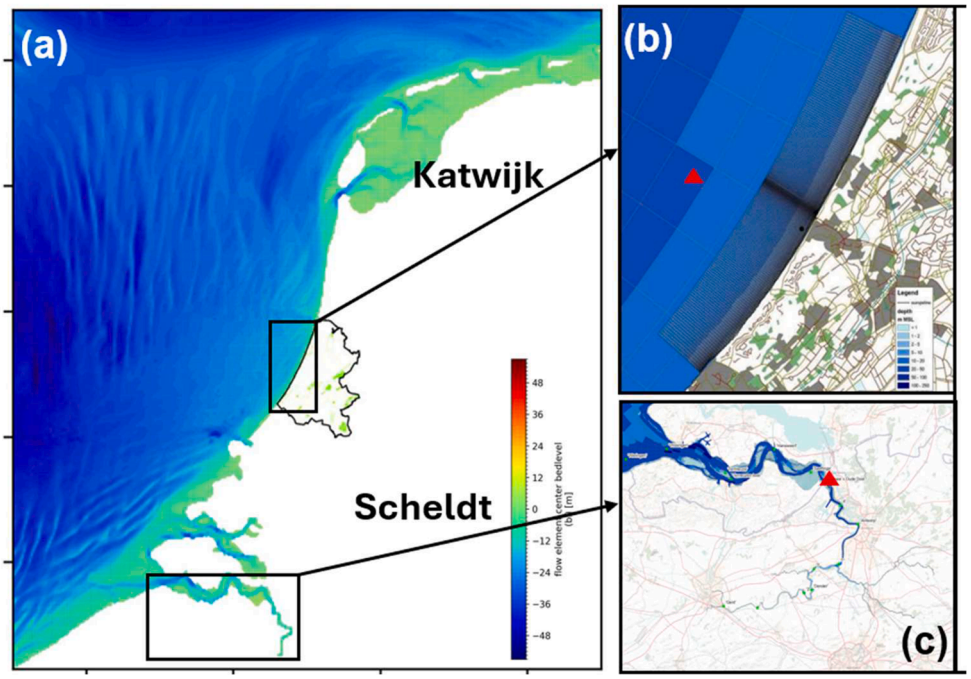

Fig. 2. Location in the Netherlands of the sites (red triangles) where model forcing conditions for the box models have been derived (b) for Katwijk and (c) Scheldt.

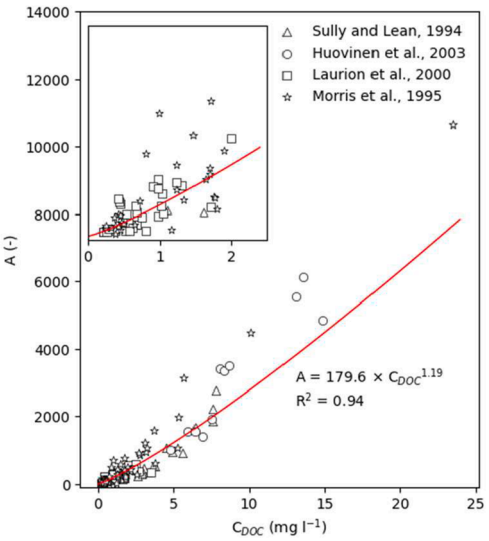

Fig. 3. Relation between DOC concentration and amplitude (insert shows detail for $C_{DOC} < 2$ mg L^{-1}), based on published observation data.

single layer at 15 cm (Maraccini et al., 2016). Therefore, the first possibility is that the observations in these two sites with a single-layer sampling are not representative of the average concentration in the whole column.

Since both poor performance results happened in winter, another explanation could be the influence of the seasonal variation of terrestrial input. Pillar Point Harbor, Arroyo Burro, and San Joaquin Marsh represent marine, brackish, and freshwater sites, respectively. Compared to Pillar Point and Arroyo Burro, San Joaquin Marsh is more vulnerable to land-based impacts (Maraccini et al., 2016). Terrestrial input, from catchments and wastewater treatment plants, can strongly impact the composition of CDOM in receiving waters (Bogard et al., 2019; Wilkinson et al., 2013). However, the variation of UV absorption capacity, triggered by the changing CDOM composition (Twardowski et al., 2004), was ignored in our model. We have s_e as a parameter to adjust the impact from CDOM compositions in the M0 module, but set as a constant value so far. s_e could be parameterized by users for specific regions in future applications.

3.2. Die-off model comparison

According to the comparisons of die-off rates between different simulations and observations (Maraccini et al., 2016 and Nguyen et al., 2015) (Fig. 5), the prediction from our M0 module was better than existing approaches (M1 and M2) based on the Root Mean Squared Error (RMSE) and R-Squared (R^2) (details in S2). The M1 module (Fig. 5b, e), which calculated the die-off rate without photo-inactivation damage, highly underestimated the observed die-off rates. The results from the M1 module (without radiation) only varied in a narrow range, between 0 and 2 day^{-1}. On the contrary, using visible light intensity to quantify photo-inactivation damage (M2, with visible light radiation) significantly overestimated the die-off rates (Fig. 5c, f, h).

As shown in Fig. 5g-h, the fluctuation of total radiation at water surfaces varied between 200 and 300 W m^{-2}, which is a considerably narrow range compared to the seasonal variation in other regions (Iqbal, 2012). Besides, there was no distinct relation between total radiation at surface water and observed/modelled die-off rates. For DOC, Fig. 5I

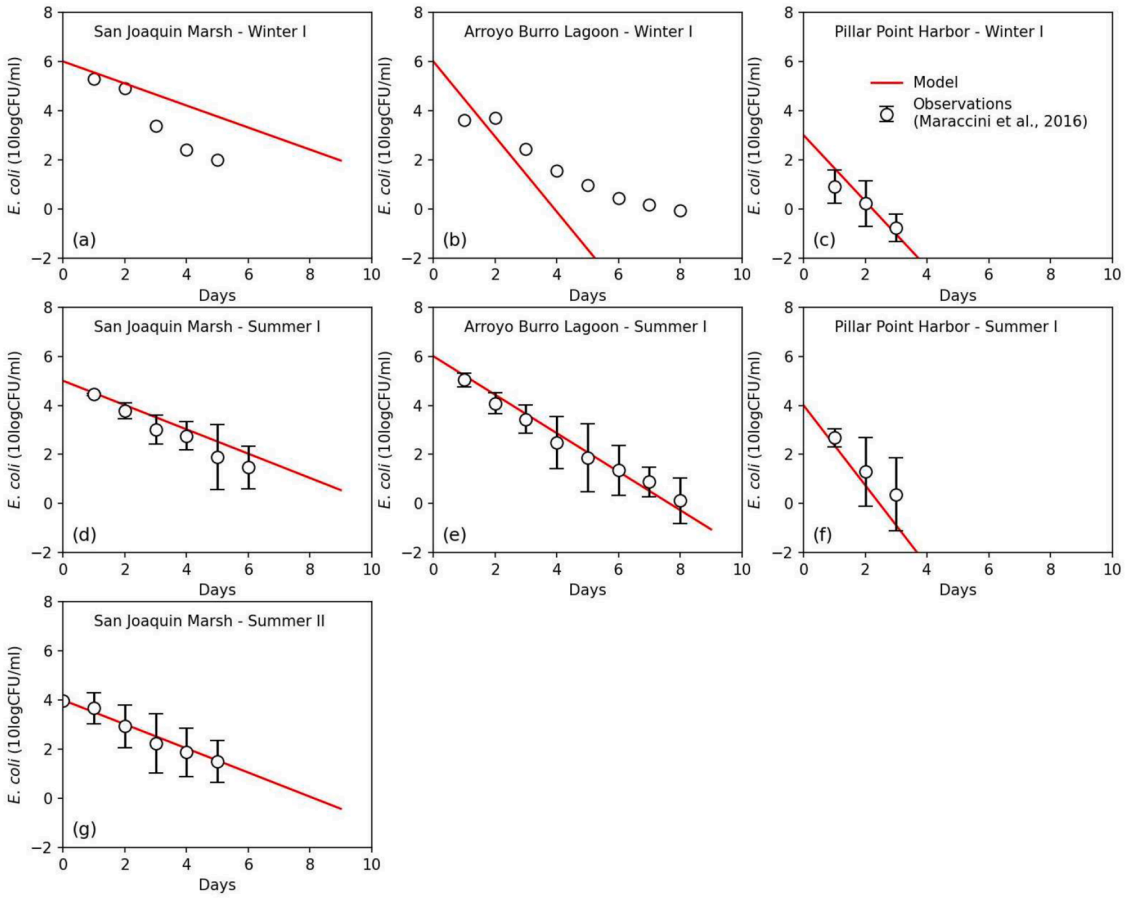

Fig. 4. Validation of the die-off module (M0) in three sites (a-c in winter; d-g in summer. Observations from Maraccini et al., 2016).

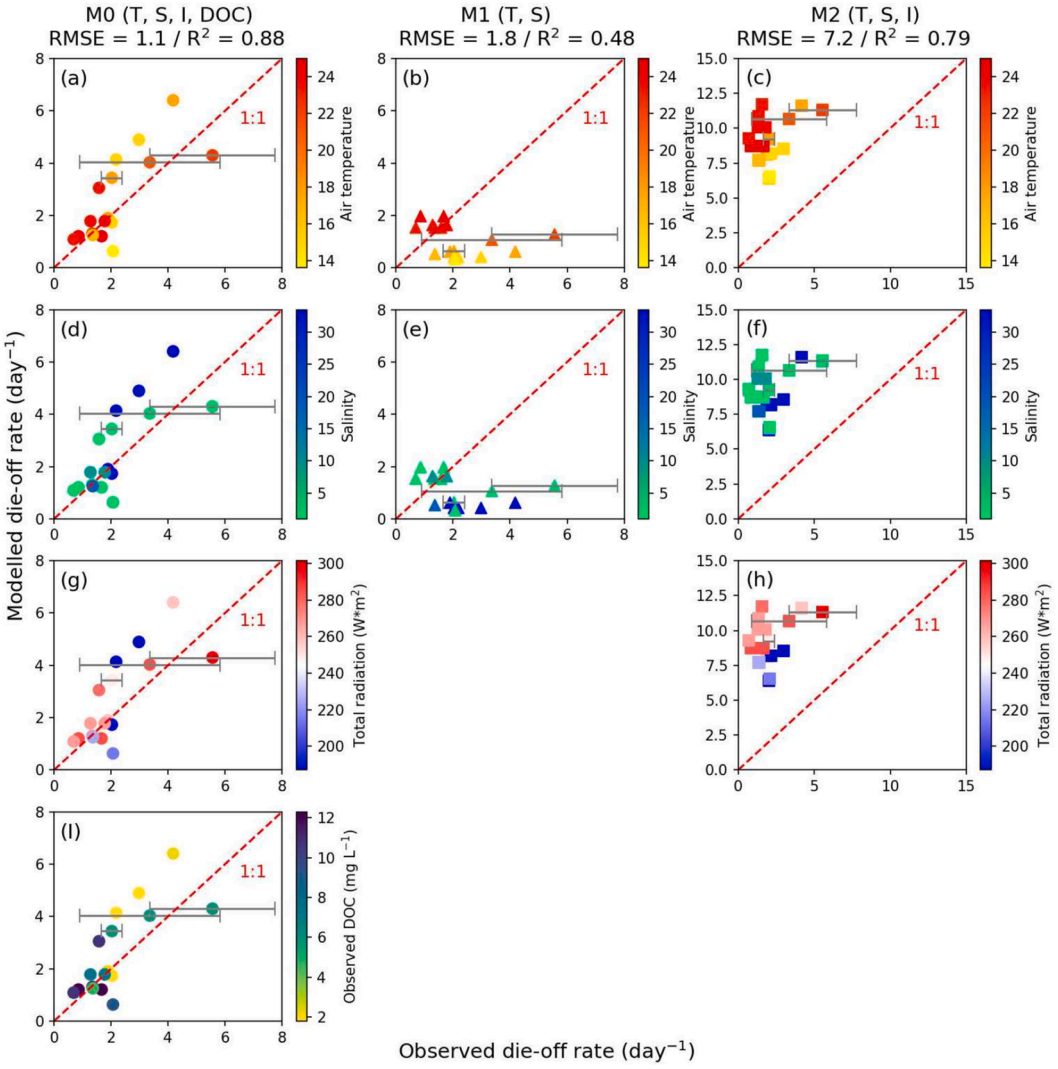

Fig. 5. Comparison of the die-off modules. Symbols, circles in (a), (d), (g), triangles in (b) and (c) and squares in (c), (f) and (h) represent the results from M0, M1 and M2, respectively. Observations are from (Maraccini et al., 2016 and Nguyen et al., 2015). Error bars show ± one standard error of duplicates.

shows that the highest DOC concentrations (dark purple) are associated with the lowest die-off rates. These indicate that in a region with less seasonal fluctuation of solar radiation but high fluctuation of DOC, *E. coli* photo-inactivation is highly correlated with light absorption of CDOM.

Water temperature and salinity cannot be used to predict the die-off rate solely (M1), especially in low-temperature periods (Fig. 5b). However, when high DOC concentration (> 6 mg L^{-1}) restricts the penetration of light, modelled die-off rates from M0 are in a similar range (0 – 2 day^{-1}) to the predictions from M1. This suggests that in waters rich in CDOM, the impact of photo-inactivation is less distinguishable. This is probably why the M1 module has been widely used for modelling *E. coli* die-off rate in small catchments and wetlands (De Brauwere et al., 2014a; Niazi et al., 2015; Sowah et al., 2020; Worku Meshesha et al., 2020) where the CDOM concentration is usually high (Seitzinger et al., 2005).

On the contrary, solar radiation is essential for calculating *E. coli* die-off rate in "clearer" coastal waters (Chan et al., 2015; Gao et al., 2015; Huang et al., 2015, 2017; Thupaki et al., 2013), but calculating the photo-induced damage as a linear function of total radiation and neglecting the extinction by CDOM (as in the M2 model, Fig. 5h) overestimated the *E. coli* die-off rate. CDOM concentrations in coastal waters have seasonal patterns due to riverine input and in situ primary production (Zweifel et al., 1995), which can induce a significant impact on *E. coli* die-off variation.

3.3. Validation of sediment interaction module

Few studies measured suspended sediment attached *E. coli* due to sampling uncertainty (Devane et al., 2020). Therefore, we used the *E. coli* distribution between waters and sediments from previous studies to validate the sediment interaction module (Section 2.4) (Devane et al., 2020; Fluke et al., 2019; Kim et al., 2010; Labite et al., 2010; Pachepsky and Shelton, 2011). Observed ratios of *E. coli* concentrations in waters versus in deposited sediments ranged from 2:1 (10th percentile) to 1263:1 (90th percentile) (Fig. 6a). S5 (dynamic sediment partitioning coefficient, K_{SS_D}) simulations yielded ratios of 11:1–281:1, within the observed 10th - 90th percentiles (Fig. 6b). The average ratio from S5_Katwijk was 66:1, which was higher than that from the S5_Scheldt (14:1), resulting from a higher clay proportion in the Katwijk model (**Figure S4**). In contrast, the ratio in S4_Katwijk (3265:1) was lower than in S5_Scheldt (4797:1) (Fig. 6c). Besides, the K_{SS_C} allocated more *E. coli* into the deposited sediment, leading to a ratio up to 14,791:1, well above the 90th percentile of observations.

The comparison in Fig. 6b indicates that using clay and non-clay components is a reasonable approach for modeling *E. coli* attachment-detachment. The K_{SS_C} value used in S4 (0.01 m^3), commonly applied

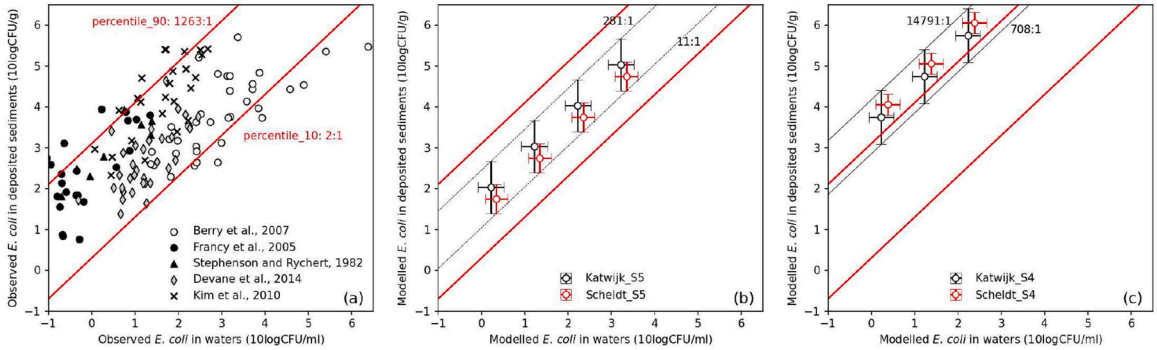

Fig. 6. *E. coli* concentrations in waters vs sediments collected from previous studies (a) and from the box models S5 with K_{SS_D} (b) and S4 with K_{SS_C} (c). The Error bars mean fluctuation within a year. The red lines represent the 10th (2:1) and 90th (1263:1) percentiles of the observed ratios. The black lines represent the maximum and minimum ratios from the simulation results.

in previous models (Bai and Lung, 2005; Gao et al., 2011; Thupaki et al., 2013), appears too high for *E. coli* attachment (Fig. 6c). Direct K_{SS} measurements are rare, only limited groundwater studies reported the K_{SS} values between 1×10^{-4} and 1×10^{-6} m^3 g^{-1} (Gantzer et al., 2001; Lindqvist and Enfield, 1992; Reddy and Ford, 1996). This range was consistent with the K_{SS_D} simulation by the box models **(Figure S4)**, but two to four orders of magnitude lower than the K_{SS_C}. In addition, using K_{SS_C} also ignored the impact of TSS composition on *E. coli* attachment.

3.4. Sensitivity analysis

In our long-term scenarios (S1-S5, Table 1), scenario S2 (without CDOM extinction) predicted lower *E. coli* concentrations than the other scenarios (Fig. 7). As discussed in Section 3.2, ignoring the extinction by CDOM can overestimate the UV-induced damage, whereas including CDOM extinction (S3) reduces radiation effects. The Scheldt_S3 concentrations were similar to the Scheldt_S1 (T-test, $P = 4.39$, details in S2) (Fig. 7b) due to high DOC concentrations and aligned seasonal patterns of DOC concentration and radiation **(Figure S3)**. These indicate that the UV penetration is too low to inactivate *E. coli*. This explains why temperature alone can "adequately" predict *E. coli* in catchments with high DOC concentrations (De Brauwere et al., 2014a; Niazi et al., 2015; Sowah et al., 2020; Worku Meshesha et al., 2020). However, Katwijk_S1 showed 44 % higher average unattached *E. coli* concentration than Katwijk_S3 (Fig. 7a), highlighting the importance of UV inactivation in clear waters with low DOC concentrations (Chan et al., 2015; Gao et al., 2015; Huang et al., 2015, 2017; Thupaki et al., 2013).

The concentrations in S5 were very similar to S3 (T-test, $P = 4.01$ for Katwijk; 2.83 for Scheldt). Since the long-term scenarios represent a steady baseflow/low-flow period (Table 2), *E. coli* concentrations in waters and in sediments remain in equilibrium. As a result, sediment interaction has no visible effect in the long-term sensitivity analysis.

In the short-term sensitivity analysis (E1-E4, Table 1), E4 (including interactions with sediment) had a bigger tail than the other scenarios (Fig. 8). This extended tail appeared in both summer and winter and started earlier in the Scheldt_E4. Due to high turbidity, the event duration in Scheldt_S4 was prolonged by 29–44 h compared to E3 in both seasons. In Katwijk, the difference among E1, E2, and E3 was significant, but the difference between E3 and E4 above the threshold was insignificant (Fig. 8a-b).

As mentioned in 2.3, the short-term sensitivity analysis simulated peak *E. coli* pollution events. Since no sediment interaction was involved in E1–3, deposited sediment could not accumulate and release *E. coli* during and after the peak event. In E4, higher TSS in the Scheldt created a larger *E. coli* reservoir in deposited sediment than in Katwijk_E4 during peak events, leading to greater post-event release. The longer exceedance in Scheldt_E4 shows that sediment interaction can extend the *E. coli* pollution above the threshold by roughly 30 h after a peak. To prevent the post-event pollution and warn bathers of a potential extended risk, sediment interaction could be included in *E. coli* forecasts for highly turbid waters, especially during peak events.

3.5. Model limitations and applications

Model validation and comparison with the existing models indicated that the new model can give a more reliable prediction of photo-inactivation and distribution of *E. coli* between waters and sediments. Incorporating UV spectrum, DOC and suspended sediment concentrations for photo-inactivation calculation improved the dynamics of prediction. The introduction of the dynamic partitioning coefficient added the effect of suspended sediment composition on the attachment process. However, the new model requires additional inputs (Table 2,

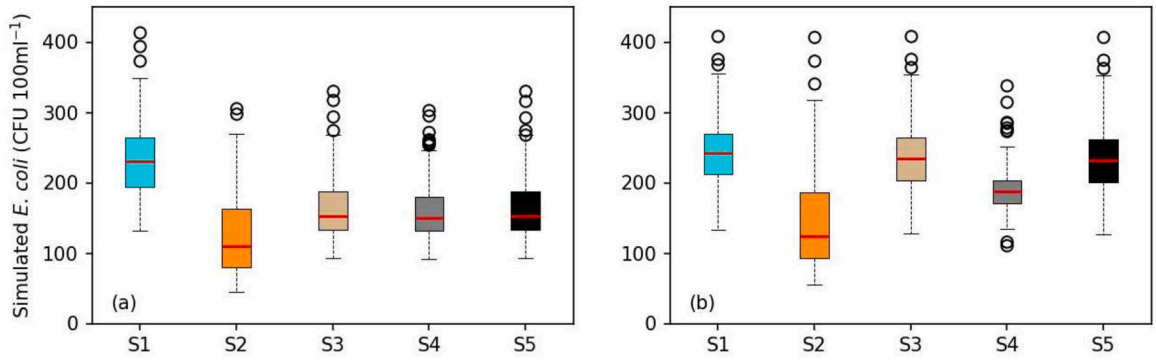

Fig. 7. Long-term sensitivity analysis: unattached *E. coli* concentration simulations from Katwijk_S1-Katwijk_S5 (a) and from Scheldt_S1-Scheldt_2 (b). The scenarios are in Table 1.

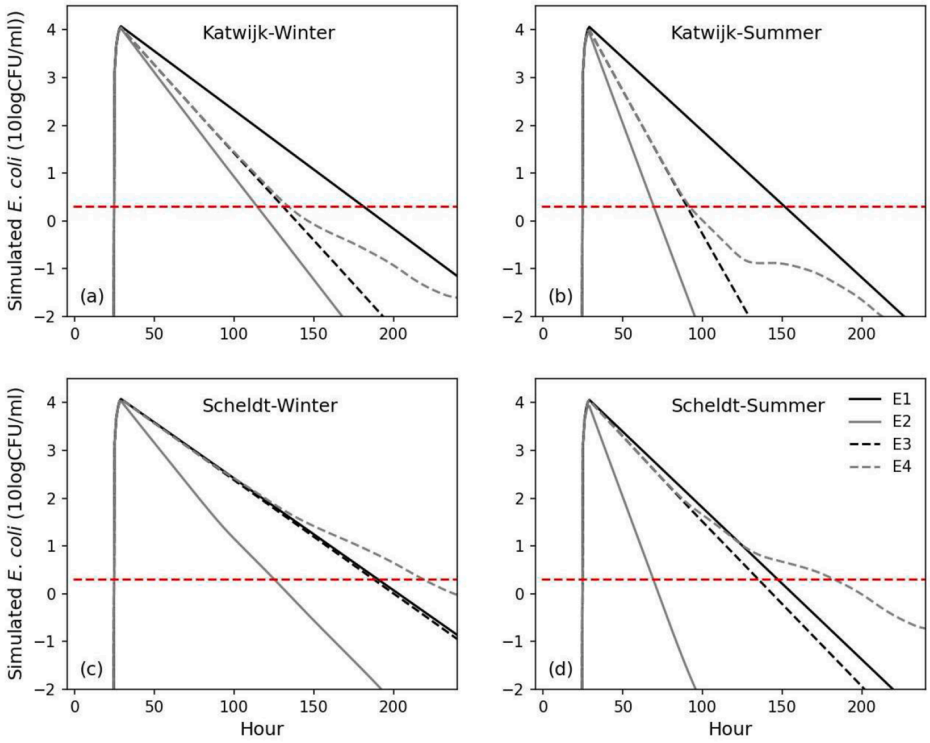

Fig. 8. Short-term sensitivity analysis. The Katwijk box model results for winter (a) and summer (b); The Scheldt model results for winter (c) and summer (d). The red dashed line is 250 CFU $100ml^{-1}$. E1–4 represents the scenarios in Table 1.

Table S2) and increases model complexity. Besides, variability of CDOM composition may affect UV extinction, but is not yet included in the box models. The correlation between K_{ss} and P_{clay} was based on a regression model from a previous study and requires more observational data in future studies. Currently, the new model has been validated only in box models, instead of in whole hydrology/hydrodynamics model domains. Future applications could integrate it with 1D/2D/3D hydrology and hydrodynamics models at various temporal-spatial scales. Parameters listed in Table S1 could be re-parameterized for other fecal bacteria or viruses with similar processes to *E. coli*. Future work is planned on applying our new *E. coli* model to a coupling model (inland 1D hydrology model + nearshore 3D hydrodynamic model) to forecast *E. coli* and support bathing water management across the source-to-sea system.

4. Conclusions

A new FIB physico-biochemical model has been developed to predict *E. coli* concentrations in natural waters and support bathing water management. It consists of a die-off module and a sediment interaction module, including the independent natural die-off, photo-inactivation, UV extinction, attachment-detachment, sedimentation, resuspension, and hyporheic exchange. The main conclusions from model validation, comparison and sensitivity analysis are as follows:

(1) The new die-off module has a lower RMSE value (1.1 day^{-1}) and a higher R^2 value (0.88) than the existing models (1.8–7.2 day^{-1}, and 0.48–0.79), indicating an improvement in agreement with observations. However, the validation dataset remains limited. It is recommended that future studies provide comprehensive FIB die-off data alongside relevant environmental factors.
(2) The model comparisons showed that photo-inactivation is crucial for estimating *E. coli* die-off rate, and CDOM extinction coefficient plays a key role in determining UVA + UVB extinction while DOC concentration is below ~6 mg L^{-1}.
(3) Sediment interaction module using dynamic partitioning coefficient produced the water-sediment *E. coli* distribution ratio within the observed 10th-90th percentile range, while the module using constant partitioning coefficient overestimated the ratio.
(4) Sensitivity analysis suggested that sediment release after a peak event can extend the pollution to roughly 30 h in highly turbid waters. Therefore, sediment interaction should be considered in *E. coli* modelling and forecasting.

Given the high flexibility of the model, it can be coupled with hydrology and hydrodynamic models and applied to FIB modelling in various bathing waters. Based on the sensitivity analysis, we also recommend different process options for different aquatic systems. This new model offers a reliable tool for predicting pathogen risk in near-future forecasting and climate change projections to support bathing safety management.

CRediT authorship contribution statement

Hao Wang: Writing – original draft, Methodology, Data curation, Conceptualization. **Anouk Blauw:** Writing – review & editing, Supervision, Methodology, Conceptualization. **Jos van Gils:** Methodology, Conceptualization. **Eline Boelee:** Writing – review & editing, Supervision. **Émile Sylvestre:** Writing – review & editing, Supervision. **Gertjan Medema:** Writing – review & editing, Supervision, Methodology.

Declaration of competing interest

The authors declare that they have no known competing financial interests or personal relationships that could have appeared to influence the work reported in this paper.

Acknowledgments

The authors thank Marieke Eleveld for support with the UV extinction setup. This research has been supported through the BlueAdapt Project which has received funding from the European Union's Horizon Europe research and innovation programme under grant agreement No 101057764 and by the UKRI/HM Government.

Supplementary materials

Supplementary material associated with this article can be found, in the online version, at doi:10.1016/j.watres.2025.125199.

Data availability

Data will be made available on request.

References

Annually, R.I. (1995) ASTM STANDARDS. https://doi.org/10.1520/uvcmp20170001.
Bai, S., Lung, W.-S., 2005. Modeling sediment impact on the transport of fecal bacteria. Water Res. 39, 5232–5240. https://doi.org/10.1016/j.watres.2005.10.013.
Bi, S., Hieronymi, M., Röttgers, R., 2023. Bio-geo-optical modelling of natural waters. Front. Mar. Sci. 10, 1196352. https://doi.org/10.3389/fmars.2023.1196352.
Bogard, M.J., Kuhn, C.D., Johnston, S.E., Striegl, R.G., Holtgrieve, G.W., Dornblaser, M. M., Spencer, R.G., Wickland, K.P., Butman, D.E., 2019. Negligible cycling of terrestrial carbon in many lakes of the arid circumpolar landscape. Nat. Geosci. 12, 180–185. https://doi.org/10.1038/s41561-019-0299-5.
Bricaud, A., Morel, A., Prieur, L., 1981. Absorption by dissolved organic matter of the sea (yellow substance) in the UV and visible domains. Limnol. Ocean 26, 43–53. https://doi.org/10.4319/lo.1981.26.1.0043.
Chan, Y., Thoe, W., Lee, J.H., 2015. Field and laboratory studies of *Escherichia coli* decay rate in subtropical coastal water. J. Hydro-Environ. Res. 9, 1–14. https://doi.org/10.1016/j.jher.2014.08.002.
Cho, K.H., Pachepsky, Y.A., Oliver, D.M., Muirhead, R.W., Park, Y., Quilliam, R.S., Shelton, D.R., 2016. Modeling fate and transport of fecally-derived microorganisms at the watershed scale: state of the science and future opportunities. Water Res. 100, 38–56. https://doi.org/10.1016/j.watres.2016.04.064.
De Brauwere, A., Gourgue, O., De Brye, B., Servais, P., Ouattara, N.K., Deleersnijder, E., 2014a. Integrated modelling of faecal contamination in a densely populated river–sea continuum (Scheldt River and Estuary). Sci. Total. Environ. 468, 31–45. https://doi.org/10.1016/j.scitotEnviron.2013.08.019.
de Brauwere, A., Ouattara, N.K., Servais, P., 2014b. Modeling fecal indicator bacteria concentrations in natural surface waters: a review. Crit. Rev. Environ. Sci. Technol. 44, 2380–2453. https://doi.org/10.1080/10643389.2013.829978.
Deltares, 2020. D-Water Quality User Manual. Deltares. https://oss.deltares.nl/web/delft3d/manuals.
Devane, M.L., Moriarty, E., Weaver, L., Cookson, A., Gilpin, B., 2020. Fecal indicator bacteria from environmental sources; strategies for identification to improve water quality monitoring. Water Res. 185, 116204. https://doi.org/10.1016/j.watres.2020.116204.
Enns, A.A., Vogel, L.J., Abdelzaher, A.M., Solo-Gabriele, H.M., Plano, L.R., Gidley, M.L., Phillips, M.C., Klaus, J.S., Piggot, A.M., Feng, Z., 2012. Spatial and temporal variation in indicator microbe sampling is influential in beach management decisions. Water Res. 46, 2237–2246. https://doi.org/10.1016/j.watres.2012.01.040.
Erichsen, A.C., Kaas, H., Dannisøe, J., Mark, O., Jørgensen, C., 2006. Etablering af badevandsprofiler og varslingssystemer i henhold til EU's nye badevandsdirektiv. Miljøstyrelsen Og DHI. Miljøprojekt.
Fichot, C.G., Benner, R., 2011. A novel method to estimate DOC concentrations from CDOM absorption coefficients in coastal waters. Geophys. Res. Lett. 38. https://doi.org/10.1029/2010gl046152.
Fluke, J., González-Pinzón, R., Thomson, B., 2019. Riverbed sediments control the spatiotemporal variability of *E. coli* in a highly managed, arid river. Front. Water. 1, 4. https://doi.org/10.3389/frwa.2019.00004.
Gantzer, C., Gaspard, P., Galvez, L., Huyard, A., Dumouthier, N., Schwartzbrod, J., 2001. Monitoring of bacterial and parasitological contamination during various treatment of sludge. Water Res. 35, 3763–3770. https://doi.org/10.1016/s0043-1354(01)00105-1.
Gao, G., Falconer, R.A., Lin, B., 2011. Numerical modelling of sediment–bacteria interaction processes in surface waters. Water Res. 45, 1951–1960. https://doi.org/10.1016/j.watres.2010.12.030.
Gao, G., Falconer, R.A., Lin, B., 2015. Modelling the fate and transport of faecal bacteria in estuarine and coastal waters. Mar. Pollut. Bull. 100, 162–168. https://doi.org/10.1016/j.marpolbul.2015.09.011.
Garcia-Armisen, T., Servais, P., 2009. Partitioning and fate of particle-associated *E. coli* in river waters. Water. Environ. Res. 81, 21–28. https://doi.org/10.2175/106143008x304613.
Garzio-Hadzick, A., Shelton, D., Hill, R., Pachepsky, Y., Guber, A., Rowland, R., 2010. Survival of manure-borne *E. coli* in streambed sediment: effects of temperature and sediment properties. Water Res. 44, 2753–2762. https://doi.org/10.1016/j.watres.2010.02.011.
Gonsior, M., Zwartjes, M., Cooper, W.J., Song, W., Ishida, K.P., Tseng, L.Y., Jeung, M.K., Rosso, D., Hertkorn, N., Schmitt-Kopplin, P., 2011. Molecular characterization of effluent organic matter identified by ultrahigh resolution mass spectrometry. Water Res. 45, 2943–2953. https://doi.org/10.1016/j.watres.2011.03.016.
Graczyk, T.K., Sunderland, D., Awantang, G.N., Mashinski, Y., Lucy, F.E., Graczyk, Z., Chomicz, L., Breysse, P.N., 2010. Relationships among bather density, levels of human waterborne pathogens, and fecal coliform counts in marine recreational beach water. Parasitol. Res. 106, 1103–1108. https://doi.org/10.1007/s00436-010-1769-2.
Hipsey, M.R., Antenucci, J.P., Brookes, J.D., 2008. A generic, process-based model of microbial pollution in aquatic systems. Water. Resour. Res. 44 (7). https://doi.org/10.1029/2007wr006395.
Huang, G., Falconer, R.A., Lin, B., 2015. Integrated river and coastal flow, sediment and *Escherichia coli* modelling for bathing water quality. Water. (Basel) 7, 4752–4777. https://doi.org/10.3390/w7094752.
Huang, G., Falconer, R.A., Lin, B., 2017. Integrated hydro-bacterial modelling for predicting bathing water quality. Estuar. Coast. Shelf. Sci. 188, 145–155. https://doi.org/10.1016/j.ecss.2017.01.018.
Huovinen, P., Penttilä, H., Soimasuo, M., 2003. Spectral attenuation of solar ultraviolet radiation in humic lakes in Central Finland. Chemosphere 51, 205–214. https://doi.org/10.1016/s0045-6535(02)00634-3.
Iqbal, M., 2012. An Introduction to Solar Radiation. Elsevier. https://doi.org/10.1016/b978-0-12-373750-2.50017-3.
Jerlov, N.G. (2014) Optical oceanography. https://doi.org/10.1016/s0422-9894(08)x7043-6.
Jozić, S., Cenov, A., Glad, M., Peroš-Pucar, D., Kurić, K., Puljak, T., Ordulj, M., Tomaš, A. V., Baumgartner, N., Ivanković, D., 2024. The effect of sampling frequency and spatial and temporal variation in the density of fecal indicator bacteria on the assessment of coastal bathing water quality. Water Res. 264, 122192. https://doi.org/10.1016/j.watres.2024.122192.
Kalev, S., Duan, S., Toor, G.S., 2021. Enriched dissolved organic carbon export from a residential stormwater pond. Sci. Total. Environ. 751, 141773. https://doi.org/10.1016/j.scitotEnviron.2020.141773.
Kim, J.-W., Pachepsky, Y.A., Shelton, D.R., Coppock, C., 2010. Effect of streambed bacteria release on *E. coli* concentrations: monitoring and modeling with the modified SWAT. Ecol. Modell. 221, 1592–1604. https://doi.org/10.1016/j.ecolmodel.2010.03.005.
Kim, M., Boithias, L., Cho, K.H., Silvera, N., Thammahacksa, C., Latsachack, K., Rochelle-Newall, E., Sengtaheuanghoung, O., Pierret, A., Pachepsky, Y.A., Ribolzi, O., 2017. Hydrological modeling of fecal indicator bacteria in a tropical mountain catchment. Water Res. 119, 102–113. https://doi.org/10.1016/j.watres.2017.04.038.
King, J., Ahmadian, R., Falconer, R.A., 2021. Hydro-epidemiological modelling of bacterial transport and decay in nearshore coastal waters. Water Res. 196, 117049. https://doi.org/10.1016/j.watres.2021.117049.
Kondo, T., Sakai, N., Yazawa, T., Shimizu, Y., 2021. Verifying the applicability of SWAT to simulate fecal contamination for watershed management of Selangor River, Malaysia. Sci. Total. Environ. 774, 145075. https://doi.org/10.1016/j.scitotEnviron.2021.145075.
Kuhn, P., Browman, H., McArthur, B., St-Pierre, J.F., 1999. Penetration of ultraviolet radiation in the waters of the estuary and Gulf of St. Lawrence. Limnol. Ocean 44, 710–716. https://doi.org/10.4319/lo.1999.44.3.0710.
Labite, H., Lunani, I., van der Steen, P., Vairavamoorthy, K., Drechsel, P., Lens, P., 2010. Quantitative Microbial risk analysis to evaluate health effects of interventions in the urban water system of Accra, Ghana. J. Water. Health 8, 417–430. https://doi.org/10.2166/wh.2010.021.
Laurion, I., Ventura, M., Catalan, J., Psenner, R., Sommaruga, R., 2000. Attenuation of ultraviolet radiation in mountain lakes: factors controlling the among-and within-lake variability. Limnol. Ocean 45, 1274–1288. https://doi.org/10.4319/lo.2000.45.6.1274.
Li, J., Yu, Q., Tian, Y.Q., Boutt, D.F., 2018. Effects of landcover, soil property, and temperature on covariations of DOC and CDOM in inland waters. J. Geophys. Res. 123, 1352–1365. https://doi.org/10.1002/2017jg004179.
Lindqvist, R., Enfield, C.G., 1992. Biosorption of dichlorodiphenyltrichloroethane and hexachlorobenzene in groundwater and its implications for facilitated transport. Appl. Environ. Microbiol. 58, 2211–2218. https://doi.org/10.1128/aem.58.7.2211-2218.1992.
Maraccini, P.A., Wenk, J., Boehm, A.B., 2016. Photoinactivation of eight health-relevant bacterial species: determining the importance of the exogenous indirect mechanism. Environ. Sci. Technol. 50, 5050–5059. https://doi.org/10.1021/acs.est.6b00074.s001.
Morel, A., Gentili, B., Claustre, H., Babin, M., Bricaud, A., Ras, J., Tieche, F., 2007. Optical properties of the "clearest" natural waters. Limnol. Ocean 52, 217–229. https://doi.org/10.5194/bg-4-1041-2007.
Morris, D.P., Zagarese, H., Williamson, C.E., Balseiro, E.G., Hargreaves, B.R., Modenutti, B., Moeller, R., Queimalinos, C., 1995. The attenuation of solar UV radiation in lakes and the role of dissolved organic carbon. Limnol. Ocean 40, 1381–1391. https://doi.org/10.4319/lo.1995.40.8.1381.
Nelson, K.L., Boehm, A.B., Davies-Colley, R.J., Dodd, M.C., Kohn, T., Linden, K.G., Liu, Y., Maraccini, P.A., McNeill, K., Mitch, W.A., 2018. Sunlight-mediated inactivation of health-relevant microorganisms in water: a review of mechanisms and modeling approaches. Environ. Sci. Process. Impacts 20, 1089–1122. https://doi.org/10.1039/c8em00047f.
Nguyen, M.T., Jasper, J.T., Boehm, A.B., Nelson, K.L., 2015. Sunlight inactivation of fecal indicator bacteria in open-water unit process treatment wetlands: modeling

endogenous and exogenous inactivation rates. Water Res. 83, 282–292. https://doi.org/10.1039/c8em00047f.
Niazi, M., Obropta, C., Miskewitz, R., 2015. Pathogen transport and fate modeling in the Upper Salem River Watershed using SWAT model. J. Environ. Manage. 151, 167–177. https://doi.org/10.1016/j.jenvman.2014.12.042.
Ouattara, N.K., de Brauwere, A., Billen, G., Servais, P., 2013. Modelling faecal contamination in the Scheldt drainage network. J. Mar. Syst. 128, 77–88. https://doi.org/10.1016/j.jmarsys.2012.05.004.
Pachepsky, Y., Shelton, D., 2011. *Escherichia coli* and fecal coliforms in freshwater and estuarine sediments. Crit. Rev. Environ. Sci. Technol. 41, 1067–1110. https://doi.org/10.1080/10643380903392718.
Reddy, H.L., Ford, R.M., 1996. Analysis of biodegradation and bacterial transport: comparison of models with kinetic and equilibrium bacterial adsorption. J. Contam. Hydrol. 22, 271–287. https://doi.org/10.1016/0169-7722(95)00095-x.
Scully, N., Lean, D., 1994. The attenuation of ultraviolet radiation in temperate lakes. Ergeb. Limnol. 43, 135. -135.
Seitzinger, S.P., Harrison, J.A., Dumont, E., Beusen, A.H., Bouwman, A., 2005. Sources and delivery of carbon, nitrogen, and phosphorus to the coastal zone: an overview of Global Nutrient Export from watersheds (NEWS) models and their application. Glob. Biogeochem. Cycles 19. https://doi.org/10.1029/2005gb002606.
Shi, X., Jovanovic, D., Meng, Z., Hipsey, M.R., McCarthy, D., 2024. Modelling faecal microbe dynamics within stormwater constructed wetlands. Water Res. 248, 120855. https://doi.org/10.1016/j.watres.2023.120855.
Shifrin, K., 1998. Physical Optics of Ocean Water. American Institute of Physics, Melville, NY. https://doi.org/10.1016/0021-9797(88)90136-1.
Silverman, A.I., Guest, J.S., 2022. Cleaner water with light. Nat. Sustain. 5, 737–738. https://doi.org/10.1038/s41893-022-00926-4.
Silverman, A.I., Nelson, K.L., 2016. Modeling the endogenous sunlight inactivation rates of laboratory strain and wastewater *E. coli* and enterococci using biological weighting functions. Environ. Sci. Technol. 50, 12292–12301. https://doi.org/10.1021/acs.est.6b03721.
Smith, R.C., Baker, K.S., 1981. Optical properties of the clearest natural waters (200–800 nm). Appl. Opt. 20, 177–184. https://doi.org/10.1364/ao.20.000177.
Sowah, R.A., Bradshaw, K., Snyder, B., Spidle, D., Molina, M., 2020. Evaluation of the soil and water assessment tool (SWAT) for simulating *E. coli* concentrations at the watershed-scale. Sci. Total. Environ. 746, 140669. https://doi.org/10.1016/j.scitotEnviron.2020.140669.
Sterk, A., Schijven, J., de Nijs, T., de Roda Husman, A.M., 2013. Direct and indirect effects of climate change on the risk of infection by water-transmitted pathogens. Environ. Sci. Technol. 47, 12648–12660. https://doi.org/10.1021/es403549s.
Stolte, W., Schueder, R., 2019. Update of the Water Quality Model Application of the Schelde for the Year 2014 - Calibration and Validation 64. https://vnsc.eu/publicaties/archief/update-of-the-water-quality-model-application-of-the-schelde-for-the-year-2014/.
Stramski, D., Babin, M., Woźniak, S.B., 2007. Variations in the optical properties of terrigenous mineral-rich particulate matter suspended in seawater. Limnol. Ocean 52, 2418–2433. https://doi.org/10.4319/lo.2007.52.6.2418.
Thorndahl, S., Nielsen, J.M., Rasmussen, M.R., 2024. Model-based prediction of bathing water quality in a lake polluted by fecal coliform bacteria from combined sewer overflows. J. Environ. Manage. 349, 119483. https://doi.org/10.1016/j.jenvman.2023.119483.
Thupaki, P., Phanikumar, M.S., Schwab, D.J., Nevers, M.B., Whitman, R.L., 2013. Evaluating the role of sediment-bacteria interactions on *Escherichia coli* concentrations at beaches in southern Lake Michigan. J. Geophys. Res. Oceans 118, 7049–7065. https://doi.org/10.1002/2013jc008919.
Tong, X., Goh, S.G., Mohapatra, S., Tran, N.H., You, L., Zhang, J., He, Y., Gin, K.Y.-H., 2024. Predicting antibiotic resistance and assessing the risk burden from antibiotics: a holistic modeling framework in a tropical reservoir. Environ. Sci. Technol. 58, 6781–6792. https://doi.org/10.1021/acs.est.3c10467.
Twardowski, M.S., Boss, E., Sullivan, J.M., Donaghay, P.L., 2004. Modeling the spectral shape of absorption by chromophoric dissolved organic matter. Mar. Chem. 89, 69–88. https://doi.org/10.1016/j.marchem.2004.02.008.
van Loosdrecht, M.C., Lyklema, J., Norde, W., Zehnder, A.J., 1989. Bacterial adhesion: a physicochemical approach. Microb. Ecol. 17, 1–15. https://doi.org/10.1007/bf02025589.
Wang, J., Seyed-Yagoobi, J., 1994. Effects of water turbidity and salt concentration levels on penetration of solar radiation under water. Sol. Energy 52, 429–438. https://doi.org/10.1016/0038-092x(94)90120-q.
Wilkinson, G.M., Pace, M.L., Cole, J.J., 2013. Terrestrial dominance of organic matter in north temperate lakes. Glob. Biogeochem. Cycles 27, 43–51. https://doi.org/10.1029/2012gb004453.
Worku Meshesha, T., Wang, J., Demelash Melaku, N., 2020. A modified hydrological model for assessing effect of pH on fate and transport of *Escherichia coli* in the Athabasca River basin. J. Hydrol. 582, 124513. https://doi.org/10.1016/j.jhydrol.2019.124513.
Zhang, Y., Shi, K., Zhou, Q., Zhou, Y., Zhang, Y., Qin, B., Deng, J., 2020. Decreasing underwater ultraviolet radiation exposure strongly driven by increasing ultraviolet attenuation in lakes in eastern and southwest China. Sci. Total. Environ. 720, 137694. https://doi.org/10.1016/j.scitotEnviron.2020.137694.
Zhang, Z., Li, B., Li, N., Sardar, M.F., Song, T., Zhu, C., Lv, X., Li, H., 2019. Effects of UV disinfection on phenotypes and genotypes of antibiotic-resistant bacteria in secondary effluent from a municipal wastewater treatment plant. Water Res. 157, 546–554. https://doi.org/10.1016/j.watres.2019.03.079.
Zijl, F., Verlaan, M., Gerritsen, H., 2013. Improved water-level forecasting for the Northwest European Shelf and North Sea through direct modelling of tide, surge and non-linear interaction. Ocean. Dyn. 63, 823–847. https://doi.org/10.1007/s10236-013-0624-2.
Zweifel, U.L., Wikner, J., Hagström, Å., Lundberg, E., Norrman, B., 1995. Dynamics of dissolved organic carbon in a coastal ecosystem. Limnol. Ocean 40, 299–305. https://doi.org/10.4319/lo.1995.40.2.0299.